RSC Advances

PAPER

Cite this: *RSC Adv.*, 2018, **8**, 12165

Understanding differences in Er^{3+}–Yb^{3+} codoped glass and glass ceramic based on upconversion luminescence for optical thermometry

Yingxin Hao,[a] Shichao Lv,[a] Zhijun Ma[a] and Jianrong Qiu *[ab]

Received 8th February 2018
Accepted 21st March 2018

DOI: 10.1039/c8ra01245h

rsc.li/rsc-advances

Optical thermometry has attracted growing consideration due to its outstanding performance. In this research, precursor glass with compositions of $50SiO_2$–$20Al_2O_3$–$30CaF_2$–$0.5ErF_3$–$1YbF_3$ and the corresponding CaF_2 glass ceramic were prepared for optical temperature sensing comparison. A large enhancement in upconversion luminescence originated from thermally coupled energy levels ($^2H_{11/2}$ and $^4S_{3/2}$) and $^4F_{9/2}$ was confirmed in the transparent glass ceramic (GC). Importantly, the temperature-dependent upconversion fluorescence intensity ratios of glass and GC were investigated from 303 K to 573 K under a 980 nm laser with constant pumping power. It was found that GC shows weaker optical thermometry ability than the precursor glass in terms of temperature sensitivity, the maximum relative sensitivity of GC reached to 10.6×10^{-3} K^{-1} at 303 K while that of the glass is 11.15×10^{-3} K^{-1} at 303 K, the thermally coupled energy gap reduced about 34.2 cm^{-1} after crystallization, we attribute this change to the crystal field effect. Furthermore, the FIR value variation of glass shows weaker pumping power dependence than GC in terms of thermal effect induced by laser. The temperature-cycle measurements suggest that both glass and GC exhibit favorable thermal stability. Consequently, our results may contribute to enriching our understanding of the optical temperature sensing properties of glass and glass ceramic in other systems and provide a comprehensive perspective to design practical optical thermometry materials.

Introduction

Life is closely linked with the temperature, whether it is macroscopic ambient temperature or microscopic life activities, temperature monitoring is extremely significant in many applications.[1–5] Recently, a new non-contact temperature sensor, optical thermometry, has attracted growing interest due to possessing superior properties such as high sensitivity, rapid response time and immunity to harsh environment when compared to traditional contact thermometers.[6–8] The temperature-sensitive optical techniques based on fluorescence lifetime and fluorescence intensity ratio (FIR) are two main mechanisms, relevant investigations concentrate on transition metal (TM)[9–11] ions and rare earth (RE)[12–15] ones. Notably, benefited from self-calibrated capacity and high reliability, improved measurement accuracy,[16,17] FIR technique has been widely applied to determine temperature and regarded as a promising way for optical thermometry. It makes use of emission bands from thermally coupled energy levels (TCEL), the ratio of which can avoid the influences originated from spectral losses and fluctuations in excitation intensity.[14,15,18,19] So far, the materials that have thermally coupled energy levels are rare earth ions,[12,14,20–22] for instance, Er^{3+}, Tm^{3+}, Ho^{3+}, Eu^{3+}, Sm^{3+}.

Especially, Er^{3+} ion is one of most studied sensitive probe in optical temperature sensing,[13,15,22–24] which ascribes to remarkable fluorescence intensities change from thermally coupled energy levels (TCEL) consisting of $^2H_{11/2}$ and $^4S_{3/2}$, as a sensitizer, Yb^{3+} is always adopted as codoped ion to improve upconversion emission. Within the last few decades, optical thermometry based on FIR technique in non-crystalline materials doped with Er^{3+} have been growingly investigated, such as glass systems,[25–29] oxyfluoride glass ceramic.[13,16,22,24,30] Generally, transparent oxyfluoride glass ceramic exhibits more excellent luminescence property than glass for combining the merits of oxide glass' good stability and fluoride nanocrystals' low phonon energy environment.[31,32] Additionally in terms of temperature sensing, hosts with lower phonon energy will show higher luminescence efficiencies, which will contribute to improving measurement accuracy,[22,33] thus various glass ceramic materials for optical thermometry are widely explored currently. However, as we know, the energy gap between two thermally coupled levels will make a big difference on

[a]State Key Laboratory of Luminescent Materials and Devices, Institute of Optical Communication Materials, South China University of Technology, Guangzhou 510641, China

[b]State Key Laboratory of Modern Optical Instrumentation, College of Optical Science and Engineering, Zhejiang University, Hangzhou 310027, China. E-mail: qjr@scut.edu.cn

temperature sensitivity in fact, the improvement of luminescence efficiencies and measurement accuracy has no necessary relation with elevation of temperature sensitivity, and it is also ambiguous that what influence the different crystal field of glass ceramic has on rare earth ions' thermally coupled levels after crystallization. Therefore, understanding variation about temperature sensitivity in glass and glass ceramic is greatly essential to design optical thermometry materials with optimized properties. Unfortunately, the report concerning comparison on temperature sensing property between them is scarce, as far as we know.

In this sense, Er^{3+}–Yb^{3+} codoped silicate glass and transparent oxyfluoride glass ceramic were successfully prepared by conventional melt-quenching method and successive heat treatment. Their structural, photoluminescence properties and temperature-dependent optical behaviors were systematically investigated to explore the possible application based on FIR technique. It was found that, compared to glass, glass ceramic show stronger upconversion luminescence and higher measurement accuracy while the temperature sensitivity decreased to a certain extent after crystallization, and in the aspect of thermal effect induced by 980 nm NIR laser, the upconversion emission spectra of glass show a weaker pumping power dependence than glass ceramic, finally, both of them exhibit favorable thermal stability. All results may provide comprehensive way to design practical optical thermometry materials.

Experimental procedure

The glass sample was prepared with the following composition (mol%): $50SiO_2$–$20Al_2O_3$–$30CaF_2$–$1YbF_3$–$0.5ErF_3$ in an electric furnace (with MoS_2 heating elements) by the conventional melt-quenching method. A 30 g reagent-grade mixture of SiO_2 (99.99%), Al_2O_3 (99.99%) CaF_2 (99.9%), YbF_3 (99.99%) and ErF_3 (99.99%) was mixed thoroughly in an agate mortar and melted in a covered corundum crucible at 1450 °C for 40 min. The glass samples were fabricated by pouring the melt into a preheated stainless steel plate and then pressed it into a slice with another cool iron plate immediately, then the precursor glasses were annealed at 400 °C for 2 h to release inner stress and cool to room temperature naturally. Finally based on the thermal analysis result, glass slices with the thickness of 2 mm were cut and heat-treated at 650 °C for 2 h to obtain transparent glass ceramic (GC).

The crystal structures of prepared GC samples were determined by X-ray diffraction (XRD, PANalytical, Netherlands) with Cu/K_α ($\lambda = 0.1541$ nm) radiation in the 2 Theta range from 10° to 90°. The morphology and crystal size of the nanocrystals in glass-ceramic were obtained by high-resolution transmission electron microscope (HRTEM, 2100F, JEOL, Japan), GC samples were ground into a very fine powder which was placed onto a carbon coated copper grid and introduced into the microscope. Upconversion fluorescence measurement of the as-prepared glass and GC was investigated on a Triax (iHR 320, JobinYvon, France) fluorescence spectrometer with an adjustable fiber laser (980 nm) as the excitation. Temperature-dependent luminescence measurements of glass and GC were recorded on the same fluorescence spectrometer with a home-made temperature controlling apparatus and a 980 nm laser by means of designing light path.

Results and discussion

To identify the amorphous state and crystalline phase in precursor glass and GC, samples were ground into powders for XRD measurement, as is shown in Fig. 1. There is no any sharp diffraction peaks in precursor glass due to high cooling rate. In contrast, several specific diffraction peaks are detected in the GC pattern after heat treatment, and the sharp peaks appeared in GC match well with the diffraction peaks of CaF_2 (PDF no. 00-035-0816) crystal. These characteristic peaks at $2\theta = 28.2°$, 47°, 55.7°, 68.6°, 75.8°, 87.3° are all ascribed to the diffractions of the (111), (220), (311), (400), (331) and (422) crystal facets of CaF_2, respectively. Meanwhile, no other sharp peaks were observed in the XRD pattern of GC, which indicates that only CaF_2 crystals are precipitated after the heat treatment.

TEM and HRTEM are measured to intuitively confirm the precipitation of CaF_2 crystals in silicate glass after heat treatment, as is presented in Fig. 2(a) lots of darker particles dispersed in the glassy matrix with average crystal diameters about 7 nm. According to Rayleigh scattering theory, the transmission loss caused by light scattering is negligible when the emission wavelength of upconversion is much larger than the size of crystals. Thus it can be inferred the optical transmission loss in GC cannot be affected seriously for application compared with precursor glass. Fig. 2(b) illustrates the HRTEM image of an individual nanoparticle. The crystal lattice fringes is very obvious and spacing d values of about 0.158 nm are assigned to the (222) crystal facets of the cubic face structure of CaF_2 crystal. Additionally from the inset of Fig. 2(a), the pattern consists of amorphous diffuse rings and some bright diffraction spots from CaF_2 crystalline grain. All these results indicate that only CaF_2 nanocrystals have successfully precipitated in the silicate glass.

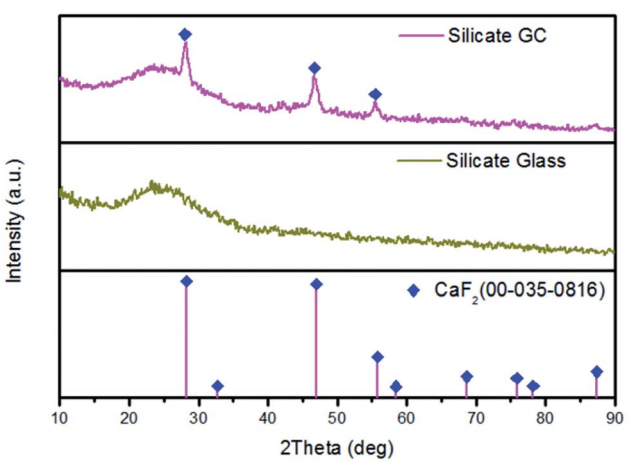

Fig. 1 XRD patterns of the precursor glass and GC after heat treatment for 2 h at 650 °C.

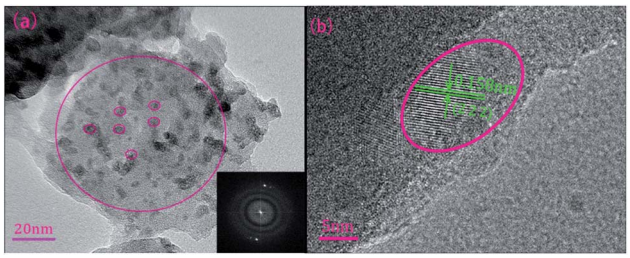

Fig. 2 (a) TEM micrograph of the GC sample and corresponding SAED patterns. (b) HRTEM micrograph of an individual CaF_2 nanoparticle in silicate GC.

Fig. 3 displays the visible upconversion emission spectra of glass and glass ceramic under 980 nm laser excitation at room temperature. The emissions spectra in glass and GC are composed of several peaks located at 525 nm ($^2H_{11/2} \rightarrow {}^4I_{15/2}$), 547 nm ($^4S_{3/2} \rightarrow {}^4I_{15/2}$) and 660 nm ($^4F_{9/2} \rightarrow {}^4I_{15/2}$), the green emission bands originated from $^2H_{11/2}$ and $^4S_{3/2}$ which is the thermally coupled energy levels will be responsible for temperature-dependent luminescence. Obviously, both emission intensity of green and red bands of GC increased enormously compared to that of precursor glass, thus it can be inferred that rare earth ions have been located in CaF_2 crystal field, and the enhancement of luminescence intensity could be ascribed to the lower phonon energy environment and local symmetry site of CaF_2 crystal. Notably, the upconversion spectra of GC appeared some sharp overlapping peaks, which is due to that Stark energy level splitting occurred in Er^{3+} under the effect of crystal field, the phenomenon also demonstrate rare earth ions have been contained in CaF_2 crystals. Compared with precursor glass, these results confirm the luminescence emission efficiency of GC have been improved remarkably after rare earth ions participate in CaF_2 crystal field.

The inset of Fig. 3 presents possible upconversion mechanisms, when excited by 980 nm laser, Er^{3+} at $^4I_{15/2}$ ground state

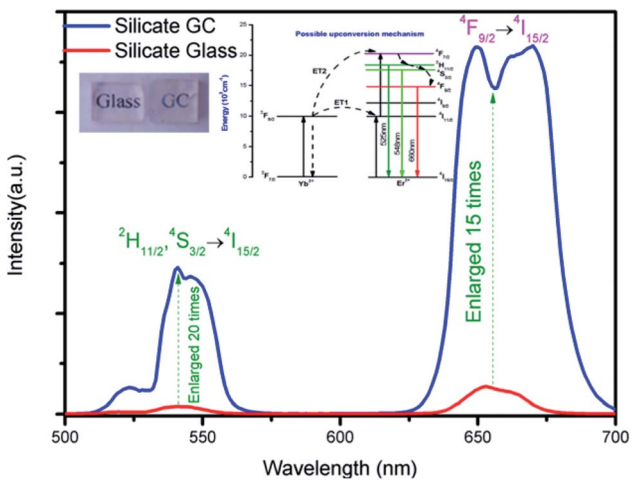

Fig. 3 Upconversion spectra of Er^{3+}–Yb^{3+} codoped silicate glass and glass ceramic under excitation of 980 nm laser, the insets exhibit energy level diagrams of Er^{3+}–Yb^{3+}, possible upconversion mechanisms and photographs of glass and GC.

are firstly pumped to $^4I_{11/2}$ intermediate excited state by ground state absorption, subsequently, the excited-state $^4I_{11/2}$ level of Er^{3+} can be populated to higher emitting levels $^4F_{7/2}$ by means of two most common excitation processes: (a) ESA, where an excited Er^{3+} ion absorbs a second 980 nm photon, raising the electrons to the highest energy level immediately, and (b) energy transfer[34] (ET) of $^2F_{5/2}$ (Yb^{3+}) + $^4I_{11/2}$ (Er^{3+}) $\rightarrow$ $^2F_{7/2}$ (Yb^{3+}) + $^4F_{7/2}$ (Er^{3+}). Then excited electrons in the $^4F_{7/2}$ level of Er^{3+} non-radioactively relax to lower $^2H_{11/2}$, $^4S_{3/2}$, $^4F_{9/2}$ immediately after the previous population, which produce the final green emissions and red emission by radioactive transitions of $^2H_{11/2}$ $\rightarrow$ $^4I_{15/2}$ (525 nm) and $^4S_{3/2} \rightarrow {}^4I_{15/2}$ (547 nm) and $^4F_{9/2} \rightarrow {}^4I_{15/2}$ (660 nm) respectively.

The temperature-dependent normalized green upconversion spectra of precursor glass collected at different temperature from 303 K to 573 K under 980 nm excitation with constant 340 mW are shown in Fig. 4(a). It is obvious that the luminescence intensity ratio of 525 nm *versus* 547 nm increases monotonously as the temperature raises, which is due to the increased population of $^2H_{11/2}$ level at the expensive of that of $^4S_{3/2}$ level by thermally coupled.

Based on the two thermally coupled level following the Boltzmann distribution, namely $^2H_{11/2}$ and $^4S_{3/2}$, the FIR of two thermally coupled energy levels (TCELs) can be described as follows:

$$\mathrm{FIR} = \frac{I_H}{I_S} = \frac{N(^2H_{11/2})}{N(^4S_{3/2})} = \frac{g_H \sigma_H \omega_H}{g_S \sigma_S \omega_S} \exp\left(\frac{-\Delta E}{k_B T}\right) = C \exp\left(\frac{-\Delta E}{k_B T}\right)$$

where I, N, g, σ and ω represent the integral emission intensity, the number of ions, the degeneracy, the frequency and the spontaneous radioactive transition rate corresponding to $^2H_{11/2}$ $\rightarrow$ $^4I_{15/2}$ and $^4S_{3/2} \rightarrow {}^4I_{15/2}$ energy levels respectively; ΔE is the effective energy gap between $^2H_{11/2}$ and $^4S_{3/2}$, k_B is the Boltzmann constant, and T is the absolute temperature.[35] Note that if take the logarithmic of FIR, the expression evolves into following equation:

$$\ln(\mathrm{FIR}) = \ln C - \frac{\Delta E}{k_B T} = \beta - \alpha/T \quad (1)$$

Here there is a linear relation between ln(FIR) and T^{-1}, $\Delta E/k_B$ represents slope value in linear function. Because k_B is the Boltzmann constant, so the bigger the ΔE is, the bigger the slope becomes.

The natural logarithmic FIR about glass of emissions at 525 nm and 547 nm as a function of inverse absolute temperature is plotted in Fig. 4(b), the fitted straight line matches well with original data plots, whose result can be expressed by the following equation.

$$\ln(\mathrm{FIR}_{glass}) = 1.487 - 1023.4 T^{-1} \quad (2)$$

According to eqn (2) above, the effective energy gap in precursor glass between $^2H_{11/2}$ and $^4S_{3/2}$ can be inferred to 710.8 cm^{-1} in principle.

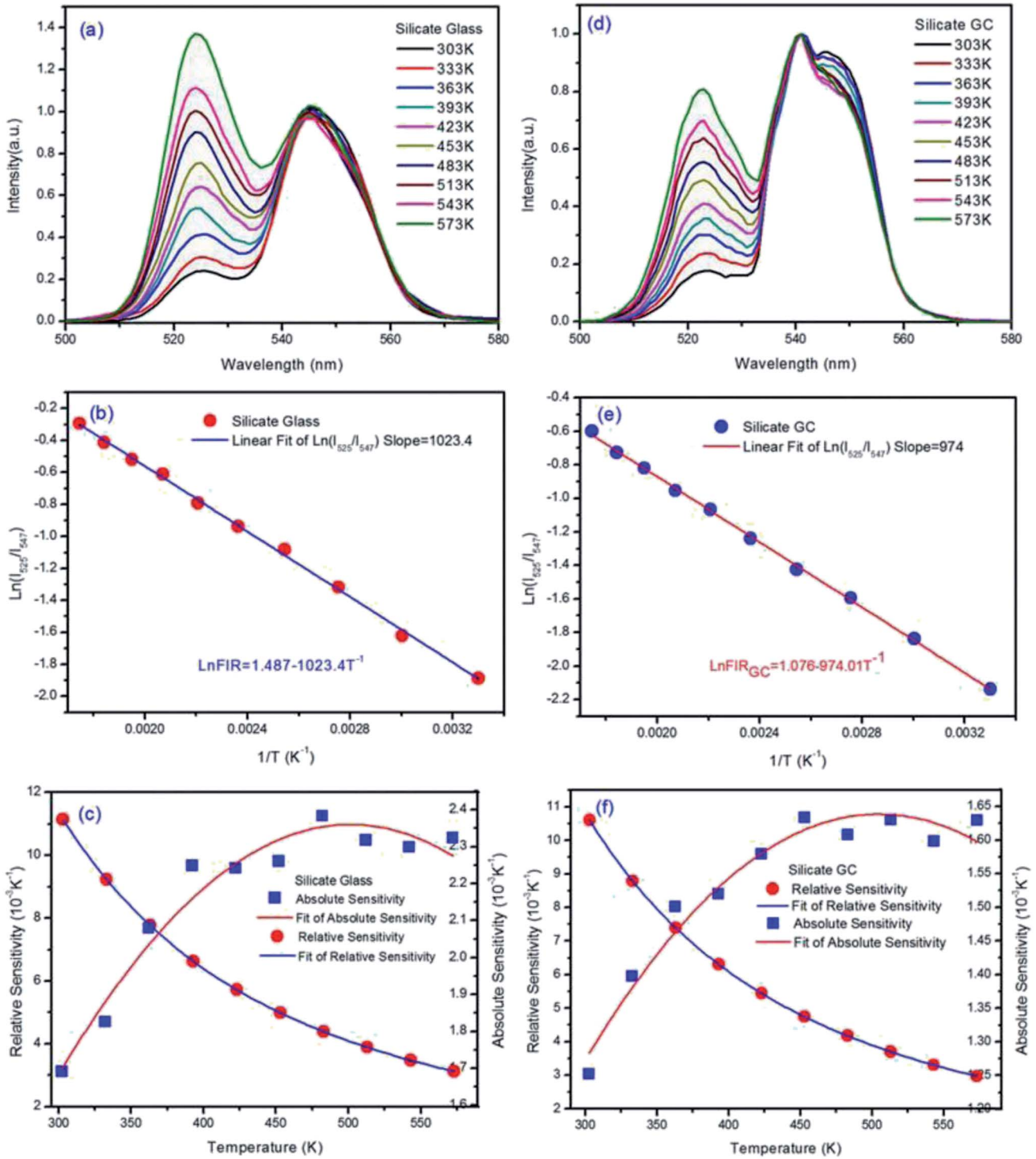

Fig. 4 (a) The normalized green upconversion spectra of glass under 980 nm laser excitation of 340 mW at various temperatures ranging from 303 K to 573 K. (b) Monolog plot about glass of the natural logarithmic FIR as a function of inverse absolute temperature. (c) Relative sensitivity S_R and absolute sensitivity S_A of precursor glass based on FIR technique at various temperatures. (d–f) Series of temperature-dependent characterization analysis of GC sample with the same condition in precursor glass.

There are two indispensible parameters evaluating the temperature sensing applications based on FIR technique, one of which is the absolute temperature sensitivity S_A and the other is relative sensitivity S_R. Actually the relative sensitivity S_R is more objective compared with the absolute temperature sensitivity because the S_A is always affected by FIR value which can be obtained diversely from materials using different procedures. The feature is reflected by their definitions:

$$S_A = \frac{dFIR}{dT} = FIR\frac{\Delta E}{k_B T^2}$$

$$S_R = \frac{1}{FIR}\frac{dFIR}{dT} = \frac{\Delta E}{k_B T^2}$$

The S_R and S_A values are in proportion to the effective energy gap ΔE. According to eqn (1), $\Delta E/k_B$ represents slope value in linear function, so the slope value can represent temperature sensitivity in fact. Fig. 4(c) describes the obtained experimental data of absolute temperature sensitivity (S_A) together with relative sensitivity (S_R) and corresponding fitting curves as a function of temperature from 303 K to 573 K. It is obvious that the S_R becomes small and small as the temperature increases while the tendency of S_A keeps increasing initially and decreasing finally. Derived from original data plots, the maximum S_A and S_R of silicate glass samples are 2.38×10^{-3} K^{-1} at 483 K and 11.15×10^{-3} K^{-1} at 303 K, respectively. Especially the maximum relative sensitivity is 11.15×10^{-3} K^{-1} at 303 K, note that it will keep increasing with the temperature descending. Derived from eqn (2), the slope value (E/k_B) of fitted logarithmic FIR curve is 1023.56 ± 14.20.

The normalized upconversion spectra and series of characterization analysis of silicate GC, similar to those of precursor glass, were collected in Fig. 4(d–f). The fluorescence intensity ratio of 525 nm *versus* 547 nm also increases monotonously as the temperature raises, according to previous theoretical analysis, the logarithmic FIR about GC as a function of inverse absolute temperature is well fitted with the expression:

$$\ln(FIR_{GC}) = 1.076 - 974.01T^{-1} \quad (3)$$

From the eqn (3), the slope of GC fitted line is 974.01 ± 9.55, we can deduced that the effective energy gap in GC between $^2H_{11/2}$ and $^4S_{3/2}$ is 676.6 cm^{-1}, notably the value have changed after crystallization when compared with precursor glass. Moreover, it gets smaller than precursor glass instead of bigger. Because the slope value can represent relative temperature sensitivity, this phenomenon means that, although upconversion emission efficiency of silicate GC enhanced greatly, its relative temperature sensitivity decreased on the contrary. As we know, rare earth ions have special electronic structure, the fluorescence emission of them originated from 4f–4f orbits does not affected easily by external environment for the reason of shielding effect by 5s–5d orbit electrons. However, the cubic face structure CaF_2 crystal fields were formed in GC around rare earth ions after heat treatment, the energy level of rare earth ions will be affected still due to strong electrostatic interaction of crystal field, such as Stark energy level splitting, which can be demonstrated from the upconversion spectra in Fig. 3. According to crystal field theory, there is a J mixed effect after Stark splitting, namely different J state about spectral items mix with each other, which will result in the movement of orthocenter of J energy level. It is the same with the thermally coupled energy level ($^2H_{11/2}$ and $^4S_{3/2}$) under the effect of crystal field, the orthocenter interval in GC between $^2H_{11/2}$ and $^4S_{3/2}$ energy bands gets closer than that of precursor glass. In short, compared with glass, the relative temperature sensitivity of GC decreased a little, which could be attributed to the crystal field effect.

Then Fig. 4(f) describes the obtained experimental data about GC of S_A and S_R as a function of variable temperature. According to the experimental data plots, the maximum S_A and S_R of silicate GC samples are 1.63×10^{-3} K^{-1} at 453 K and 10.6×10^{-3} K^{-1} at 303 K, respectively. Table 1 lists the optical temperature sensing ability of glass and corresponding GC for better comparison. In conclusion, whether it is relative sensitivity or absolute sensitivity, silicate CaF_2 GC shows weaker optical thermometry ability than precursor glass in terms of temperature sensitivity.

Considering the thermal effect caused by laser excitation, the pumping power dependent upconversion emission spectra of precursor glass and GC samples at different temperature were studied in Fig. 5. If the thermal effect induced by light source is serious, the surface temperature of sample will elevate dramatically, which can cause evident error between the test temperature and practical temperature for application. From the results collected at 303 K of Fig. 5(a) and (b), as the pumping power increases from 100 mW to 900 mW, the normalized emissions spectra of silicate glass located at 525 nm ($^2H_{11/2} \rightarrow {}^4I_{15/2}$) and 547 nm ($^4S_{3/2} \rightarrow {}^4I_{15/2}$) changed slightly while that of GC varied obviously. This means the integrated emission intensities ratio in glass and GC corresponding to thermally coupled energy levels, namely FIR, will be quiet different as a function of pumping power. Meanwhile we also monitored the similar upconversion emission spectra of precursor glass and GC at 363 K for further investigation, as is displayed in Fig. 5(c) and (d), the measurement range of pumping power was adjusted from 260 mW to 900 mW because of the weaker upconversion emission in precursor glass, which could be attributed to the more drastic non-radioactive transitions at the higher temperature. Note that the variation tendencies of glass and GC at 363 K are similar to those of pumping power dependent upconversion spectra at 303 K respectively, but the influence of pumping power on upconversion emission at higher temperature become weaker, we deduced that the higher temperature environment makes the materials less sensitive to the thermal effect caused by laser.

Table 1 Optical temperature sensing ability of glass and corresponding GC and fitted parameters including measurement accuracy based on FIR technique

Sample	$S_{R\text{-}MAX}$ (10^{-3} K^{-1})	$S_{A\text{-}MAX}$ (10^{-3} K^{-1})	$\Delta E/k_B$	Standard error
Silicate glass	11.15 at 303 K	2.38 at 483 K	1023.56	14.20
Silicate GC	10.6 at 303 K	1.63 at 453 K	974.02	9.55

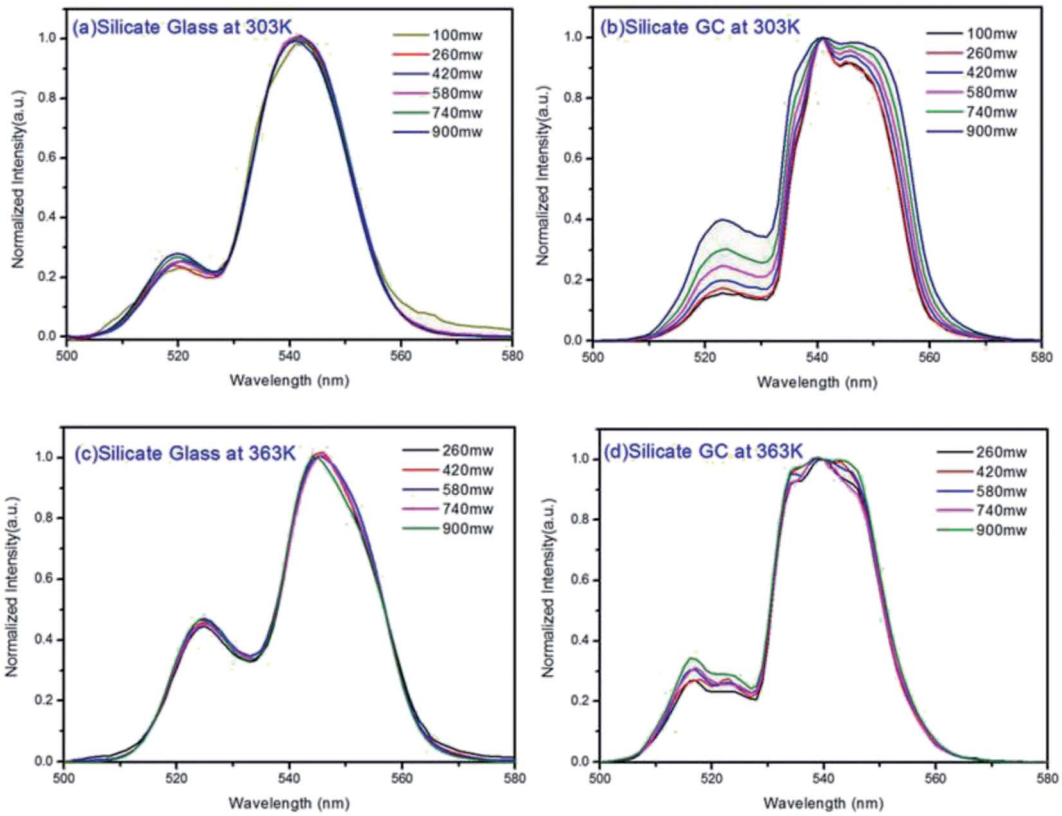

Fig. 5 (a) Pumping power dependent normalized upconversion emission spectra of precursor glass and (b) GC under 980 nm excitation at 303 K. (c and d) Pumping power dependent normalized upconversion emission spectra collected at 363 K.

Fig. 6(a) displays the pumping power dependent FIR variation in glass and GC according to Fig. 5(a) and (b) collected at 303 K. Obviously, the thermal effect have already made a difference on FIR of GC when the pumping power is above 100 mW, it increases as the pumping power rises, actually this is a big challenge for practical application of optical thermometer as the thermal effect will induce a deviation between the measured temperature and actual one. In comparison, a more favorable result is achieved in silicate glass. Note that the FIR value variation is negligible when pumping power is under 420 mW, it implies that the thermal effect in glass induced by laser within a certain power is suppressed, but with the increase continuously of pumping power, FIR value still enhanced for the reason of unavoidable thermal effect. Fig. 6(b) exhibits the result of corresponding FIR variation at 363 K based on Fig. 5(c) and (d). In terms of silicate GC, the FIR also keeps increasing initially as the pumping power rises, while the FIR value of precursor glass is basically unchanged before the pumping power reaches to 740 mW, and then it has an increasing tendency, however whether it is GC or glass, the range of FIR fluctuation induced by thermal effect at 363 K becomes smaller than that of 303 K, we attributed this difference to the less sensitivity to thermal effect when temperature increases. In conclusion, FIR value has a close relation with pumping power, therefore previous temperature-dependent green upconversion spectra of glass and GC in Fig. 4 are all monitored at the 340 mW considering the upconversion emission intensity and weaker thermal effect as much as possible. In the present samples, the FIR variation of glass induced by thermal effect shows weaker pumping power dependence than that of GC, in another word, the laser pumping power in precursor glass triggering thermal effect is much bigger than GC.

In order to measure the repeatability of the temperature dependent FIR, the thermal cycling processes between 303 K and 573 K were displayed in Fig. 7. Evidently whether it is glass or GC, FIR value at the same temperature remains almost invariable even with a process of heating and cooling, it implies that electron distribution on thermally couple energy levels can restore to their original states when cooling from 573 K to 303 K. On the other hand, the little fluctuations in FIR value of the corresponding same temperature could be ascribed to a faint

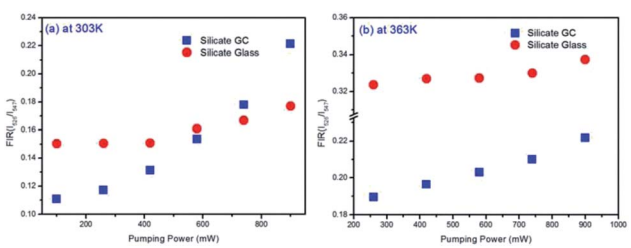

Fig. 6 (a) Comparison of pumping power dependent FIR variation in glass and GC collected at 303 K and (b) at 363 K.

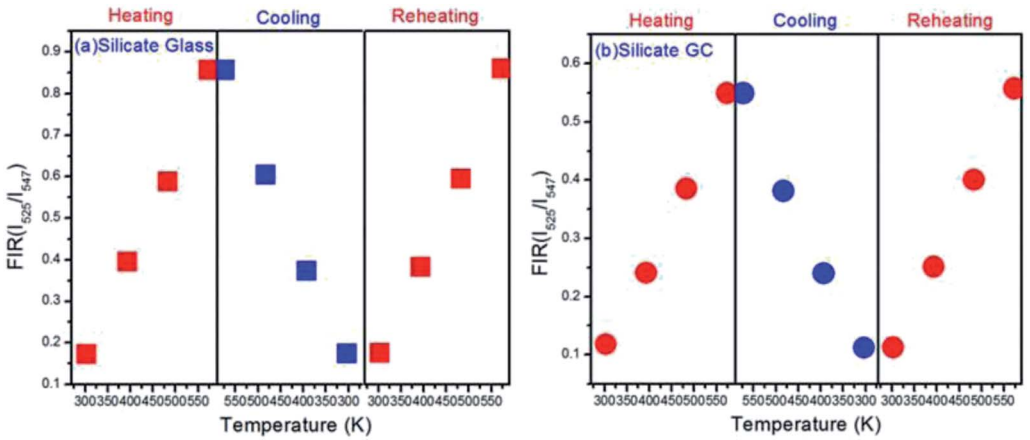

Fig. 7 (a) Plots of FIR *versus* temperature upon the thermal cycling process with the varied temperature from 303 K to 573 K in glass and (b) GC.

difference between the real temperature of measured samples and the monitoring temperature of copper heating plate. Subsequently, the FIR fluctuation is still negligible during a reheating process. These results indicate that such switching between heating and cooling of temperature dependent FIR is reversible and repeatable, we conclude that both silicate glass and GC exhibit favorable thermal stability.

Conclusion

Transparent silicate glass and corresponding CaF_2 glass ceramic were successfully fabricated, their structural, upconversion spectra and temperature-dependent luminescence measurement were investigated systematically. It was found that there are pros and cons to both of the precursor glass and glass ceramic. The upconversion luminescence intensity of GC enhanced enormously compared to that of glass. Impressively, the temperature sensitivity of GC decreased to a certain extent after crystallization, the maximum absolute sensitivity and relative sensitivity of GC reached to 1.63×10^{-3} K^{-1} at 453 K and 10.6×10^{-3} K^{-1} at 303 K, respectively, while the glass is 2.38×10^{-3} K^{-1} at 483 K and 11.15×10^{-3} K^{-1} at 303 K, it means the interval between thermally couple energy levels varied from 710.8 cm^{-1} in glass to 676.6 cm^{-1} in GC. We ascribe it to the J mixed effect of crystal field after Stark energy level splitting. Moreover, in the aspect of thermal effect induced by NIR laser, the FIR variation of glass shows weaker pumping power dependence than GC. Finally, both of glass and GC exhibit favorable thermal stability. As a consequence, these results may enrich our understanding toward the optical temperature sensing properties between glass and glass ceramic in other systems and provide comprehensive perspective to design practical optical thermometry materials.

Conflicts of interest

There are no conflicts to declare.

Acknowledgements

This work has been supported by the Guangdong Natural Science Foundation (Grants S2011030001349, 2014A030306045), and Guangdong Science and Technology Department (Grant No. 2015B090901038) and Shenzhen science & technology innovation commission (Grant No. GJHS20160330152111138).

References

1 J. Brübach, C. Pflitsch, A. Dreizler and B. Atakan, *Prog. Energy Combust. Sci.*, 2013, **39**, 37–60.
2 H. J. Seo, J. Wang, L. Qin, P. Cai, T. Vu, X. Wang, X. Yan and Y. Bu, *Opt. Lett.*, 2016, **41**, 5314–5317.
3 H. Suo, C. Guo, Z. Yang, S. Zhou, C. K. Duan and M. Yin, *J. Mater. Chem. C*, 2015, **3**, 7379–7385.
4 X. D. Wang, O. S. Wolfbeis and R. J. Meier, *Chem. Soc. Rev.*, 2013, **42**, 7834.
5 S. Zheng, W. Chen, D. Tan, J. Zhou, Q. Guo, W. Jiang, C. Xu, X. Liu and J. Qiu, *Nanoscale*, 2014, **6**, 5675.
6 X. Li, G. Jiang, S. Zhou, X. Wei, Y. Chen, C. K. Duan and M. Yin, *Sens. Actuators, B*, 2014, **202**, 1065–1069.
7 B. Dong, B. Cao, Y. He, Z. Liu, Z. Li and Z. Feng, *Adv. Mater.*, 2012, **24**, 1987.
8 Y. Tian, B. Tian, C. e. Cui, P. Huang, L. Wang and B. Chen, *Opt. Lett.*, 2014, **39**, 4164–4167.
9 D. Chen, Z. Wan and S. Liu, *Anal. Chem.*, 2016, **88**, 4099–4106.
10 D. Chen, Z. Wan and Y. Zhou, *Sens. Actuators, B*, 2016, **226**, 14–23.
11 D. Chen, Y. Zhou and Z. Wan, *Opt. Lett.*, 2015, **40**, 3607–3610.
12 Z. Cao, X. Wei, Z. Lu, Y. Chen and Y. Min, *ACS Appl. Mater. Interfaces*, 2016, **8**, 34546.
13 X. Wang, Q. Liu, P. Cai, J. Wang, L. Qin, T. Vu and H. J. Seo, *Opt. Express*, 2016, **24**, 17792.
14 S. Zhou, S. Jiang, X. Wei, Y. Chen, C. Duan and M. Yin, *J. Alloys Compd.*, 2014, **588**, 654–657.
15 A. Pandey, V. K. Rai, V. Kumar, V. Kumar and H. C. Swart, *Sens. Actuators, B*, 2015, **209**, 352–358.

16 S. Jiang, P. Zeng, L. Liao, S. Tian, H. Guo, Y. Chen, C. Duan and M. Yin, *J. Alloys Compd.*, 2014, **617**, 538–541.
17 F. Vetrone, R. Naccache, A. Zamarrón, A. Juarranz, F. Sanz-Rodríguez, L. M. Maestro, E. M. Rodríguez, D. Jaque, J. G. Sole and J. Capobianco, *ACS Nano*, 2010, **4**, 3254.
18 X. Wang, *RSC Adv.*, 2015, **5**, 86219–86236.
19 S. A. Wade, S. F. Collins and G. W. Baxter, *J. Appl. Phys.*, 2003, **94**, 4743–4756.
20 D. Chen, M. Xu, S. Liu and X. Li, *Sens. Actuators, B*, 2017, **246**, 756–760.
21 W. Xu, X. Gao, L. Zheng, Z. Zhang and W. Cao, *Sens. Actuators, B*, 2012, **173**, 250–253.
22 X. M. Li, J. K. Cao, Y. L. Wei, Z. R. Yang and H. Guo, *J. Am. Ceram. Soc.*, 2016, **98**, 3824–3830.
23 X. Cheng, K. Yang, J. Wang, L. Yang and X. Cheng, *Opt. Mater.*, 2016, **58**, 449–453.
24 D. Chen, Z. Wan, Y. Zhou, P. Huang, J. Zhong, M. Ding, W. Xiang, X. Liang and Z. Ji, *J. Alloys Compd.*, 2015, **638**, 21–28.
25 L. Feng, B. Lai, J. Wang, G. Du and Q. Su, *J. Lumin.*, 2010, **130**, 2418–2423.
26 T. Wu, R. Tong, L. Liao, L. Huang, S. Zhao and S. Xu, *Sensors*, 2017, **17**, 1253.
27 Z. Q. Feng, L. Bai, B. S. Cao, L. D. Gong and B. Dong, *Sci. China: Phys., Mech. Astron.*, 2010, **53**, 848–851.
28 W. A. Pisarski, J. Pisarska, R. Lisiecki and W. Ryba-Romanowski, *Sens. Actuators, A*, 2016, **252**, 54–58.
29 A. Pandey, S. Som, V. Kumar, V. Kumar, K. Kumar, V. K. Rai and H. C. Swart, *Sens. Actuators, B*, 2014, **202**, 1305–1312.
30 W. P. Chen, F. F. Hu, R. F. Wei, Q. G. Zeng, L. P. Chen and H. Guo, *J. Lumin.*, 2017, **192**, 303–309.
31 F. Liu, E. Ma, D. Chen, Y. Yu and Y. Wang, *J. Phys. Chem. B*, 2006, **110**, 20843–20846.
32 D. Chen, Y. Wang, Y. Yu and P. Huang, *Appl. Phys. Lett.*, 2007, **91**, 139.
33 L. Xing, W. Yang, D. Ma and R. Wang, *Sens. Actuators, B*, 2015, **221**, 458–462.
34 H. Guo and Y. M. Qiao, *Opt. Mater.*, 2009, **31**, 583–589.
35 K. Zheng, Z. Liu, C. Lv and W. Qin, *J. Mater. Chem. C*, 2013, **1**, 5502–5507.